Available online at www.sciencedirect.com

ScienceDirect

IFAC Papers Online CONFERENCE PAPER ARCHIVE

IFAC PapersOnLine 50-1 (2017) 10658–10665

Robust Generalized Dynamic Inversion Control of Autonomous Underwater Vehicles

Uzair Ansari * **Abdulrahman H. Bajodah** *

* *Aeronautical Engineering Department, King Abdulaziz University, P.O.Box 80204, Jeddah 21589, Saudi Arabia, (e-mail: abajodah@kau.edu.sa)*

Abstract: This paper presents the Robust Generalized Dynamic Inversion (RGDI) control system for Autonomous Underwater Vehicles (AUV)s. The outer (position) and the inner (attitude) loops of the control system utilize Generalized Dynamic Inversion (GDI) of two pre-specified asymptotically stable dynamics of the inertial position coordinates and the attitude angles, respectively. The outer loop provides the pitch and yaw tilting commands to the inner loop, which in turns generates values of the corresponding control surface deflections by which the vehicle's position is controlled. Sliding mode control-based elements are included in the particular parts of the two GDI control loops, and they work to robustify the GDI control system against instabilities and performance deterioration due to unmodeled nonlinearities, parametric variations, and unknown bounded disturbances. A Lyapunov stability analysis of the proposed RGDI control law is presented, and a detailed six degrees of freedom mathematical model of the Monterey Bay Aquarium Research Institute AUV is used to evaluate the controller performance. Numerical simulations are conducted under both nominal and perturbed conditions to demonstrate robustness of the control design.

Keywords: Robust Generalized Dynamic Inversion, Autonomous Underwater Vehicle, Greville Method, Lyapunov Stability, Sliding Mode Control

1. INTRODUCTION

Autonomous Underwater Vehicles (AUVs) are gaining more interest in scientific research communities because of the large benefits that they provide to mankind in both commercial and in military applications, especially those off-shore applications where human involvement is uneasy, e.g., exploring marine environment, inspection of underwater facilities, underwater lines checking, exploration of oil and mine removing missions, see Xu and Xiao (2007), Xu et al. (2006) and Yildiz et al. (2009a). Due to the harsh and dynamic environment of oceans, research has been focusing on efficiency-increasing of AUV designs and on robustifying their control systems.

The AUV control methodologies that have been proposed in the literature include linear control, see Yildiz et al. (2009b), sliding mode control, see Yang et al. (2013), Das et al. (2014), and Kim et al. (2015), fuzzy and neural network control, see Khodayari and Balochian (2015), Lakhekar et al. (2015), and Eski and Yildirim (2014).

One simple and effective nonlinear control design approach that has been implemented in marine applications is Dynamic Inversion (DI), in which the control law is formulated to eliminate system nonlinearities by means of feedback, see Subudhi and Atta (2009) and Chowdhury et al. (2014). The DI control technique in turns allows to incorporate well established linear control techniques. In despite of its flexibility and simplicity, standard DI lacks robustness to model uncertainties. Several modifications were added to the basic DI control structure to improve its robustness characteristics, see Steinicke and Michalka (2002) and Wang et al. (2012). Regardless of these attributes, DI has several shortcomings and limitations, including blind nonlinearity cancellation, large control effort, and numerical singularity configurations of square matrix inversion.

A new inversion-based control design methodology is Generalized Dynamic Inversion (GDI), see Hameduddin and Bajodah (2012) and Bajodah (2009b). The methodology is of the left inversion type, and hence it does not involve deriving inverse equations of motion for the plant. In GDI, dynamic constraints are prescribed in the form of differential equation that encapsulate the control objectives, and is generalized inverted using the Moore-Penrose Generalized Inverse (MPGI) based Greville formula, see Ben-Israel and Greville (2003) to obtain the control law for achieving desired performance. The GDI control technique has been an effective tool for several engineering problems, see Bajodah (2009a), Bajodah (2009b), Bajodah (2010), Hameduddin and Bajodah (2012) and Gui et al. (2013)).

In this paper, RGDI is proposed for position and attitude control of AUV. In the outer (position) loop, RGDI is applied to generate pitch and yaw attitude profiles based on depth and east positional errors respectively. In inner (attitude) loop, RGDI control is utilized to force the pitch and yaw attitude angles towards their desired values.

10.1016/j.ifacol.2017.08.1757

The generalized inversion singularity is avoided via a dynamic scaling factor that is augmented with the MPGI in the particular RGDI control loopTo deal with model uncertainties and external disturbances, a robustifying loop is augmented in the framework of GDI based on Sliding Mode Control (SMC). The stability of RGDI is ensured by using positive definite Lyapunov energy function. Numerical simulations are conducted on a six Degree of Freedom (DOF) simulator of the Monterey Bay Aquarium Research Institute (MBARI) AUV, see McEwen and Streitlien (2001), to analyze the performance of the proposed control algorithm.

This paper is organized as follows. Section. 2 briefly discusses the coordinate system and equations of motion of AUV. The basic formulation of GDI for the inner and outer loop is presented in section. 3. The singularity issue and its rectification is discussed in section. 4. The inclusion of robust term based on SMC is explained in Section. 5. The stability analysis of the RGDI using Lyapunov energy function is discussed in section. 6. Finally, simulation results and conclusion are presented in section. 7 and 8 respectively.

2. MATHEMATICAL MODELING

The data of the MBARI variable length AUV is shown in table 1, see McEwen and Streitlien (2001). The AUV is axially symmetric and its motion in water is controlled by an articulated ring-wing control surface with a ducted propeller. The rudder and elevator commands are executed by moving a double gimbal mechanism to actuate the ring-wing and thruster. The vehicle is stable in roll axis and hence no roll input is needed. Structural flexibility of the vehicle is not considered, and mass distribution is assumed to be uniform. The acceleration due to gravity and water density are also considered to be constants.

Table 1. MBARI specifications

Parameter	Symbol	Value	Unit
Length, L	5.554	m	
Diameter, d	0.533	m	
Mass, m	1093.1	kg	
Moment of inertia about x_B, I_x	36.677	$kg-m^2$	
Moment of inertia about y_B, I_y	2154.3	$kg-m^2$	
Moment of inertia about z_B, I_z	2154.3	$kg-m^2$	
Thrust, T_p	52.0	N	
Max. deflections of δ_θ and δ_ψ	± 15.0	deg	

2.1 Reference Frame and Coordinate Systems

The two reference frames used in deriving the AUV six DOFs equations of motion are the North-East-Depth earth-fixed frame F_E and the body-fixed frame F_B, see Figure 1. The earth-fixed coordinate system is taken to be centered at a convenient point O_E of F_E at the sea surface level. Similarly, The body-fixed coordinate system is taken to be centered at a convenient point O_B of F_B. The displacement vector from O_E to O_B is expressed in F_E as

$$\mathbf{r}_o = [x_e \;\; y_e \;\; z_e]^T_E \tag{1}$$

and the displacement vectors from O_B to the vehicle's center of gravity cg and the center of buoyancy cb are expressed in F_B as

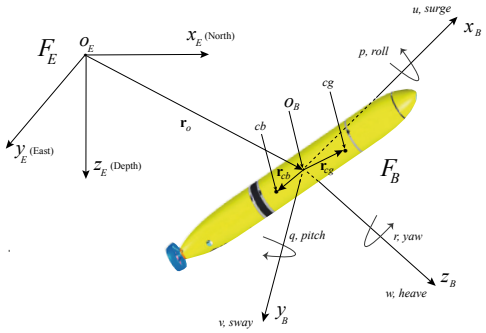

Fig. 1. Coordinate frames

$$\mathbf{r}_{cg} = [x_g \;\; y_g \;\; z_g]^T_B, \quad \mathbf{r}_{cb} = [x_b \;\; y_b \;\; z_b]^T_B. \tag{2}$$

The attitude roll, pitch, and yaw angles are denoted by ϕ, θ, and ψ, respectively. The translational surge, sway, and heave velocities of the cg are denoted in F_B by u, v, and w, and the roll, pitch, and yaw angular velocities of F_B relative to F_E are denoted in F_B by p, q, and r, respectively. The axes x_B, y_B, and z_B of the body-fixed coordinate system are chosen to form a principal positive system of axes. With this choice of body-fixed coordinates, the constants in equation (2) for the MBARI vehicle are $x_g = x_b = 12.09$ cm, $y_g = y_b = 0$, $z_g = 0.65$ cm, and $z_b = 0$. Notice that because z_g is very small compared to the dimensions of the AUV, the x_b axis is almost the longitudinal axis of the vehicle.

2.2 Kinematical Equations of Motion

The transformations between the AUV translational and rotational velocities in different reference frame determine the kinematical equations of motion, and are given by Prestero (2001); Khodayari and Balochian (2015)

$$\begin{bmatrix} \dot{x}_e \\ \dot{y}_e \\ \dot{z}_e \\ \dot{\phi} \\ \dot{\theta} \\ \dot{\psi} \end{bmatrix} = \begin{bmatrix} \mathbf{T_1} & 0_{3x3} \\ 0_{3x3} & \mathbf{T_2} \end{bmatrix} \begin{bmatrix} u \\ v \\ w \\ p \\ q \\ r \end{bmatrix} \tag{3}$$

where $\mathbf{T_1}$ and $\mathbf{T_2}$ are the transformation matrices defined as

$$\mathbf{T_1} = \begin{bmatrix} s_\psi c_\theta & c_\phi c_\psi + s_\phi s_\theta s_\psi & c_\phi s_\theta s_\psi - c_\psi s_\phi \\ c_\psi c_\theta & c_\phi s_\theta s_\psi - c_\phi s_\psi & s_\psi s_\phi - c_\phi s_\theta c_\psi \\ -s_\theta & c_\theta s_\phi & c_\phi c_\theta \end{bmatrix} \tag{4}$$

and

$$\mathbf{T_2} = \begin{bmatrix} 1 & t_\theta s_\phi & c_\phi t_\theta \\ 0 & c_\phi & -r s_\phi \\ 0 & s_\phi / c_\theta & c_\phi / c_\theta \end{bmatrix}. \tag{5}$$

where c_θ, s_θ, and t_θ refer to the trigonometric functions $\cos(\theta)$, $\sin(\theta)$, and $\tan(\theta)$, etc.

2.3 Dynamical Equations of Motion

The following are the six DOFs equations of motion for an AUV in F_B, see, e.g., McEwen and Streitlien (2001) and Prestero (2001)

$$m[\dot{u} - vr + wq - x_g(q^2 + r^2) + y_g(pq - \dot{r}) + z_g(pr + \dot{q})] = X_{ext} \tag{6}$$

$$m[\dot{v} - wp + ur - y_g(p^2 + r^2) + z_g(pr - \dot{q}) + x_g(qp - \dot{r})] = Y_{ext} \quad (7)$$

$$m[\dot{w} - uq + vp - z_g(q^2 + p^2) + x_g(pr - \dot{q}) + y_g(rq - \dot{p})] = Z_{ext} \quad (8)$$

$$I_x\dot{p} + (I_z - I_y)qr + m[y_g(\dot{w} - uq + vp) - z_g(\dot{v} - wp + ur)] = K_{ext} \quad (9)$$

$$I_y\dot{q} + (I_x - I_z)rp + m[z_g(\dot{u} - vr + wq) - x_g(\dot{w} - uq + vp)] = M_{ext} \quad (10)$$

$$I_z\dot{r} + (I_y - I_x)pq + m[x_g(\dot{v} - wp + ur) - y_g(\dot{u} - vr + wq)] = N_{ext} \quad (11)$$

where the first three equations (6-8) are the translational dynamical equations, and the second three (9-11) are the rotational dynamical equations. The right parts of the equations of motion are the components of the external forces F_{EXT} and moments M_{EXT} in F_B, comprised of

$$F_{EXT} = F_{hydrostatic} + F_{hydrodynamic} + F_{propeller} + F_{ring} \quad (12)$$

$$M_{EXT} = M_{hydrostatic} + M_{hydrodynamic} + M_{propeller} + M_{ring}. \quad (13)$$

The external forces and moments in the right hand sides of equations (6-11) are expanded as

$$X_{ext} = X_{\dot{u}}\dot{u} + X_{qq}q^2 + X_{rr}r^2 + X_{uu}u^2 + X_{vv}v^2 + X_{ww}w^2 + X_{vr}vr + X_{wq}wq - (W - B)\sin\theta + T_p\cos\delta_\psi\delta_\theta + F_x \quad (14)$$

$$Y_{ext} = Y_{\dot{r}}\dot{r} + Y_{\dot{v}}\dot{v} + Y_{wp}wp + Y_r ur + Y_v uv + Y_{v|v|}v|v| + (W - B)\cos\theta\sin\phi + T_p\sin\delta_\psi + F_y \quad (15)$$

$$Z_{ext} = Z_{\dot{q}}\dot{q} + Z_{\dot{w}}\dot{w} + Z_{vp}vp + Z_q uq + Z_w uw + Z_{w|w|}w|w| + (W - B)\cos\theta\cos\phi - T_p\cos\delta_\psi\delta_\theta + F_z \quad (16)$$

$$K_{ext} = K_{\dot{p}}\dot{p} + K_{p|p|}p|p| + (y_gW - y_bB)\cos\theta\cos\phi - (z_gW - z_bB)\cos\theta\sin\phi \quad (17)$$

$$M_{ext} = M_{\dot{q}}\dot{q} + M_{\dot{w}}\dot{w} + M_{rp}rp + M_q uq + M_w uw + M_{w|w|}w|w| + M_{q|q|}q|q| - (x_gW - x_bB)\cos\theta\cos\phi - (z_gW - z_bB)\sin\theta - x_R(F_z + T_p\cos\delta_\psi\sin\delta_\theta) \quad (18)$$

$$N_{ext} = N_{\dot{r}}\dot{r} + N_{\dot{v}}\dot{v} + N_{pq}pq + N_r ur + N_v uv + N_{r|r|}r|r| + N_{v|v|}v|v| - (x_gW - x_bB)\cos\theta\sin\phi + (y_gW - y_bB)\sin\theta + x_R(F_y + T_p\sin\delta_\psi) \quad (19)$$

where W and B are the weight of the AUV and the buoyancy force on its body, pointed to the positive and the negative z_E directions, respectively. The forces F_x, F_y, and F_z are the components of the hydrodynamic forces generated by the ring in F_B. McEwen and Streitlien (2001). All the force and moments coefficient are found in McEwen and Streitlien (2001).

3. GDI CONTROL SYSTEM DESIGN

In this paper, a two loops structure of a slow (outer) loop and a fast (inner) loop is constructed to control the under-actuated AUV, see Fig. 2. A two loop structured control is built on the fact that the attitude dynamics of the AUV is much faster than the translational dynamics. The outer loop utilizes RGDI, to generate the desired pitch and yaw θ_d and ψ_d commands based on the positional errors in depth $z_e - z_{ed}$ and east $y_e - y_{ed}$ directions respectively. The inner loop in turns solve for control deflections δ_E and δ_R required to track the desired θ_d and ψ_d attitude profiles such that the required translational trajectories are tracked. Because the roll motion of the AUV is inherently stable, the roll dynamics is not considered in the present control design.

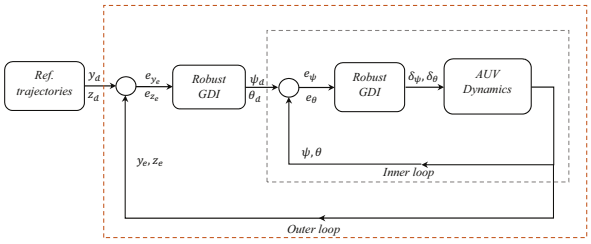

Fig. 2. Control architecture

The state vector of the AUV is given by

$$X = [x_e \;\; y_e \;\; z_e \;\; \phi \;\; \theta \;\; \psi]$$

and the control vector is $U = [\delta_\theta \;\; \delta_\psi]$. The state vector is decomposed into an inner attitude state vector x_i and an outer position state vector x_o as

$$x_i = [\theta \;\; \psi]^T, \quad x_o = [y_e \;\; z_e]^T. \quad (20)$$

3.1 GDI Formulation for Inner Attitude loop

For inner attitude dynamics, the differential equations of body Euler's angles θ and ψ is written as

$$\begin{bmatrix}\dot{\theta}\\ \dot{\psi}\end{bmatrix} = \begin{bmatrix} cos\phi & -sin\phi \\ sin\phi/cos\theta & cos\phi/cos\theta\end{bmatrix}\begin{bmatrix}q\\ r\end{bmatrix} \quad (21)$$

or

$$\dot{\mathbf{x}}_i = \mathbf{H}(\mathbf{x}_i)\mathbf{x}_r \quad (22)$$

where $\mathbf{H}(\mathbf{x}_i)$ is the lower diagonal 2×2 block of the matrix $\mathbf{T}_2$ given by (5) as

$$\mathbf{H}(\mathbf{x}_i) = \begin{bmatrix} cos\phi & -sin\phi \\ sin\phi/cos\theta & cos\phi/cos\theta\end{bmatrix} \quad (23)$$

and $\mathbf{x}_r = [q \;\; r]^T$ is the body rates state vector. The differential equations of the body rate dynamics $\dot{\mathbf{x}}_r$ is obtained by substituting the expressions of M_{ext} and N_{ext} given by (18) and (19) in (10) and (11), and solving for $\dot{q}$ and $\dot{r}$, resulting in

$$\dot{\mathbf{x}}_r = \mathbf{A}_r(\mathbf{x}_i, \mathbf{x}_r) + \mathbf{B}_r(\mathbf{x}_r)\mathbf{u}_i \quad (24)$$

where

$$\mathbf{A}_r(\mathbf{x}_i,\mathbf{x}_r)=\begin{bmatrix} -[((I_x-I_z)rp+m[z_G(\dot{u}-vr+wq) \\ -x_G(\dot{w}-uq+vp)])+M_{\dot{q}}\dot{q}+M_{\dot{w}}\dot{w}+M_{rp}rp \\ +M_q uq]/(I_y-M_{\dot{q}})+[M_w uw+M_{w|w|}w|w| \\ +M_{q|q|}q|q|-(x_GW-x_BB)cos\theta cos\phi \\ -(z_GW-z_BB)sin\theta]/(I_y-M_{\dot{q}}) \\ \\ -[((I_y-I_x)pq+m[x_G(\dot{v}-wp+ur)-y_G(\dot{u} \\ -vr+wq)])+N_{\dot{r}}\dot{r}+N_{\dot{v}}\dot{v}+N_{pq}pq \\ +N_r ur]/(I_z-N_{\dot{r}})+[N_v uv+N_{r|r|}r|r| \\ +N_{v|v|}v|v|-(x_GW-x_BB)cos\theta sin\phi \\ +(y_GW-y_BB)sin\theta]/(I_z-N_{\dot{r}}) \end{bmatrix} \tag{25}$$

$$\mathbf{B}_r(\mathbf{x}_r)=\begin{bmatrix} 0 & -T_p x_R/(I_y-M_{\dot{q}}) & 0 \\ 0 & 0 & T_p x_R/(I_z-N_{\dot{r}}) \end{bmatrix} \tag{26}$$

and

$$\mathbf{u}_i=\begin{bmatrix}\delta_\theta \\ \delta_\psi\end{bmatrix}. \tag{27}$$

The linear acceleration components $\dot{u}$, $\dot{v}$, and $\dot{w}$ in the expression of $\mathbf{A}_r$ given by (25) are accelerometer measurements obtained onboard the AUV. The inner states error vector is written as

$$\mathbf{e}_i=[e_\theta \ e_\psi]^T=[\theta-\theta_d(t) \ \psi-\psi_d(t)]^T. \tag{28}$$

The weighted error norms of attitude deviation function of AUV is defined as

$$\begin{aligned}\xi_i &= a_1(\theta-\theta_d)^2+a_2(\psi-\psi_d)^2=a_1e_\theta^2+a_2e_\psi^2 \\ &= \mathbf{e}_i^T\mathbf{D}(a_1,a_2)\mathbf{e}_i.\end{aligned} \tag{29}$$

In (29), a_1, a_2 are positive constants, $\mathbf{D}(a_1,a_2)$ denotes the diagonal matrix with diagonal elements a_1 and a_2 and the letter e denotes the error of the corresponding states from the desired values. Based on the deviation function, a linear time varying ordinary differential constraint equation is formulated, the differential order of which is the same as the relative degree of the deviation function. The equation takes the form

$$\ddot{\xi}_i+c_1(t)\dot{\xi}_i+c_2(t)\xi_i=0 \tag{30}$$

where c_1 and c_2 are chosen such that the constraint dynamic is uniformly asymptotically stable. The first and second derivatives of the constraint dynamics are calculated as

$$\dot{\xi}_i=2\mathbf{e}_i^T\mathbf{D}(a_1,a_2)(\mathbf{H}(\mathbf{x}_i)\mathbf{x}_r-\dot{\mathbf{x}}_{id}) \tag{31}$$

$$\begin{aligned}\ddot{\xi}_i=2\mathbf{e}_i^T\mathbf{D}(a_1,a_2)\{&\mathbf{H}(\mathbf{x}_i)(\mathbf{A}_r(\mathbf{x}_i,\mathbf{x}_r)+\mathbf{B}_r(\mathbf{x}_r)\mathbf{u}_i) \\ &+\dot{\mathbf{H}}(\mathbf{x}_i)\mathbf{x}_r-\ddot{\mathbf{x}}_{id}\}\end{aligned} \tag{32}$$

The function $\dot{\mathbf{H}}(\mathbf{x}_i)$ is the element-wise differentiation of $\mathbf{H}(\mathbf{x}_i)$. By placing the time derivative in the constraint dynamics described by (30), the algebraic form of constraint is written as

$$\mathbf{A}_i(\mathbf{x}_i,t)\mathbf{u}_i=B_i(\mathbf{x}_i,\mathbf{x}_r,t) \tag{33}$$

where the controls coefficient row vector function $\mathbf{A}_i$ is given by

$$\mathbf{A}_i(\mathbf{x}_i,t)=[2\mathbf{e}_i^T\mathbf{D}(a_1,a_2)\mathbf{H}(\mathbf{x}_i)\mathbf{B}_r(\mathbf{x}_r)] \tag{34}$$

and the controls load scalar function B_i is given by

$$B_i(\mathbf{x}_i,\mathbf{x}_r,t)=\begin{bmatrix} -2\mathbf{e}_i^T\mathbf{D}(a_1,a_2)(-\ddot{\mathbf{x}}_{id}+\dot{\mathbf{H}}(\mathbf{x}_i)\mathbf{H}(\mathbf{x}_i)^{-1} \\ \mathbf{x}_{id}+\mathbf{H}(\mathbf{x}_i)\mathbf{A}_r(\mathbf{x}_i,\mathbf{x}_r)-2\dot{\mathbf{e}}_i^T\mathbf{D}(a_1,a_2)\dot{\mathbf{e}}_i \\ -2c_1\mathbf{e}_i^T\mathbf{D}(a_1,a_2)\dot{\mathbf{e}}_i-c_2[a_1,a_2]\dot{\mathbf{e}}_i \end{bmatrix}. \tag{35}$$

Equation (33) is an under-determined algebraic system that has infinite number of solutions. The general solution of this system is given by the Greville formula

$$\mathbf{u}_i=\mathbf{A}_i^+(\mathbf{x}_i,t)B_i(\mathbf{x}_i,\mathbf{x}_r,t)+\mathbf{P}_i(\mathbf{x}_i,t)\boldsymbol{\lambda}_i \tag{36}$$

where $\mathcal{A}_i^+$ is the MPGI of $\mathcal{A}_i$, given by,

$$\mathcal{A}_i^+(\mathbf{x}_i,t)=\frac{\mathcal{A}_i^T(\mathbf{x}_i,t)}{\mathcal{A}_i(\mathbf{x}_i,t)\mathcal{A}_i^T(\mathbf{x}_i,t)} \tag{37}$$

$\boldsymbol{\lambda}_i\in R^2$ is null control vector defined as $\boldsymbol{\lambda}_i=\mathbf{k}_i\dot{\mathbf{e}}_\mathbf{i}{}^T$, and $\mathbf{P}_i$ is the null projection matrix given by

$$\mathbf{P}_i(\mathbf{x}_i,t)=\mathbf{I}_{2\times2}-\mathbf{A}_i^+(\mathbf{x}_i,t)\mathbf{A}_i(\mathbf{x}_i,t) \tag{38}$$

where $\mathbf{I}_{2\times2}$ is the 2×2 identity matrix. By placing the control law given by (36) in (24), the closed loop body rate dynamics is written as

$$\begin{aligned}\dot{\mathbf{x}}_r=\mathbf{A}_r(\mathbf{x}_i,\mathbf{x}_r,t)+\mathbf{B}_r(\mathbf{x}_r)\{&\mathbf{A}_i^+(\mathbf{x}_i,t)B_i(\mathbf{x}_i,\mathbf{x}_r,t) \\ &+\mathbf{P}_i(\mathbf{x}_i,t)\boldsymbol{\lambda}_i\}.\end{aligned} \tag{39}$$

3.2 GDI Formulation for Outer Position loop

Expressions for the desired east and north velocity vectors $\dot{y}_{ed}$ and $\dot{z}_{ed}$ are obtained at instantaneous values of the body velocity components u, v, and w by replacing the pitch and yaw angles θ and ψ by their commands θ_d and ψ_d in the second and third rows of (3), resulting in

$$\begin{aligned}\dot{y}_{ed}=&c_{\psi_d}c_{\theta_d}u+(c_\phi s_{\theta_d}s_{\psi_d}-c_\phi s_{\psi_d})v \\ &+(s_{\psi_d}s_\phi-c_\phi s_{\theta_d}c_{\psi_d})w\end{aligned} \tag{40}$$

$$\dot{z}_{ed}=-s_{\theta_d}u+c_{\theta_d}s_\phi v+c_\phi c_{\theta_d}w. \tag{41}$$

The two command angles are set to be $\theta_d=\theta+\Delta\theta_d$ and $\psi_d=\psi+\Delta\psi_d$, where the incremental values $\Delta\theta_d$ and $\Delta\psi_d$ are the necessary corrections to the instantaneous values of θ and ψ such that θ_d and ψ_d and the corresponding vectors $\dot{z}_{ed}$ and $\dot{y}_{ed}$ are obtained for every combination of u, v, and w. Hence, (40) and (41) become

$$\begin{aligned}\dot{y}_{ed}=&(c_{\psi+\Delta\psi_d}c_{\theta+\Delta\theta_d})u \\ &+(c_\phi s_{\theta+\Delta\theta_d}s_{\psi+\Delta\psi_d}-c_\phi s_{\psi+\Delta\psi_d})v \\ &+(s_{\psi+\Delta\psi_d}s_\phi-c_\phi s_{\theta+\Delta\theta_d}c_{\psi+\Delta\psi_d})w\end{aligned} \tag{42}$$

and

$$\dot{z}_{ed}=-s_{\theta+\Delta\theta_d}u+c_{\theta+\Delta\theta_d}s_\phi v+c_\phi c_{\theta+\Delta\theta_d}w. \tag{43}$$

The two desired translational velocity equations are now simplified via linearization about the instantaneous values of θ and ψ using the small disturbance theory, see Nelson (1998). The linearization approximations of the trigonometric functions $c_{\theta+\Delta\theta_d}$ and $s_{\theta+\Delta\theta_d}$ in $\Delta\theta_d$ are

$$\cos_l(\theta+\Delta\theta_d)=\cos\theta-\Delta\theta_d\sin\theta \tag{44}$$

$$\sin_l(\theta+\Delta\theta_d)=\sin\theta+\Delta\theta_d\cos\theta \tag{45}$$

and identical linear functions in $\Delta\psi_d$ are obtained for $c_{\psi+\Delta\psi_d}$ and $s_{\psi+\Delta\psi_d}$. Accordingly, the linear approximations of (40) and (41) are

$$\begin{bmatrix}\dot{y}_{ed} \\ \dot{z}_{ed}\end{bmatrix}=\mathbf{M}\begin{bmatrix}\Delta\theta_d \\ \Delta\psi_d\end{bmatrix}+\mathbf{N} \tag{46}$$

where

$$\mathbf{M}_{(1,1)} = -us_\theta s_\psi + vs_\phi c_\theta s_\psi + wc_\phi c_\theta s_\psi \quad (47)$$

$$\mathbf{M}_{(1,2)} = uc_\theta c_\psi + v(s_\phi s_\theta c_\psi - c_\phi s_\psi) + w(s_\phi s_\psi - c_\phi s_\theta c_\psi) \quad (48)$$

$$\mathbf{M}_{(2,1)} = -uc_\theta - vs_\theta s_\phi - ws_\theta c_\phi \quad (49)$$

$$\mathbf{M}_{(2,2)} = 0 \quad (50)$$

and

$$\mathbf{N}_{(1,1)} = uc_\theta s_\psi + v(s_\phi s_\theta s_\psi + c_\phi c_\psi) + w(s_\theta c_\phi s_\psi - s_\phi c_\psi) \quad (51)$$

$$\mathbf{N}_{(2,1)} = -us_\theta + vs_\phi c_\theta + wc_\phi c_\theta. \quad (52)$$

To construct GDI control law for the outer loop, the weighted error norms of position deviation function is defined as

$$\xi_o = a_3(y_e - y_{ed})^2 + a_4(z_e - z_{ed})^2 = a_3 e_y^2 + a_4 e_z^2 = \mathbf{e}_o^T \mathbf{D}(a_3, a_4)\mathbf{e}_o \quad (53)$$

where a_3 and a_4 are positive real constants and $\mathbf{e}_o$ is the outer state error vector given by

$$\mathbf{e}_o = [e_y \ e_z]^T = [y_e - y_{ed}(t) \ z_e - z_{ed}(t)]^T. \quad (54)$$

The first and second time derivatives of ξ_o are

$$\dot{\xi_o} = 2\mathbf{e}_o^T \mathbf{D}(a_3, a_4)\dot{\mathbf{e}}_o \quad (55)$$

and

$$\ddot{\xi_o} = 2\dot{\mathbf{e}}_o^T \mathbf{D}(a_3, a_4)\dot{\mathbf{e}}_o + 2\mathbf{e}_o^T \mathbf{D}(a_3, a_4)\ddot{\mathbf{e}}_o. \quad (56)$$

Since the relative degree of the outer subsystem is 2, a second-order linear time-varying constraint dynamics is prescribed as

$$\ddot{\xi_o} + c_3(t)\dot{\xi_o} + c_4(t)\xi_o = 0 \quad (57)$$

where coefficients $c_3(t)$ and $c_4(t)$ are chosen such that the constraint dynamics given by (57) is uniformly asymptotically stable. Substituting the expressions given by (53), (55) and (56) into (57), the constraint dynamics becomes

$$2\dot{\mathbf{e}}_o^T \mathbf{D}(a_1, a_2)\dot{\mathbf{e}}_o + 2\mathbf{e}_o^T \mathbf{D}(a_1, a_2)\ddot{\mathbf{e}}_o + 2c_1\mathbf{e}_o^T \mathbf{D}(a_1, a_2)\dot{\mathbf{e}}_o + c_2\mathbf{e}_o^T \mathbf{D}(a_1, a_2)\mathbf{e}_o = 0. \quad (58)$$

To generate expressions for the tilting commands $\Delta\psi$ and $\Delta\theta$, $\ddot{e}_o$ in (58) is evaluated along the trajectories of the resulting dynamical equations. Hence, the constraint dynamics is transformed from its differential form given by (58) to the following under-determined algebraic form

$$\mathbf{A}_o(\mathbf{x}_o, t)\mathbf{u}_o = B_o(\mathbf{x}_o, t) \quad (59)$$

where

$$\mathbf{A}_o(\mathbf{x}_o, t) = 2\mathbf{e}_o^T \mathbf{D}(a_3, a_4)\mathbf{M}, \quad (60)$$

$$B_o(\mathbf{x}_o, t) = 2\mathbf{e}_o^T \mathbf{D}(a_1, a_2)\left[\ddot{\mathbf{x}}_o - \mathbf{N}\right] + 2\dot{\mathbf{e}}_o^T \mathbf{D}(a_1, a_2)\dot{\mathbf{e}}_o + 2c_1\mathbf{e}_o^T \mathbf{D}(a_1, a_2)\dot{\mathbf{e}}_o + c_2\mathbf{e}_o^T \mathbf{D}(a_1, a_2)\mathbf{e}_o \quad (61)$$

and

$$\mathbf{u}_o = \begin{bmatrix} \Delta\psi \\ \Delta\theta \end{bmatrix}. \quad (62)$$

The minimum norm solution of (59) is given by

$$\mathbf{u}_o = \mathbf{A}_o^+(\mathbf{x}_o, t)B_o(\mathbf{x}_o, t) \quad (63)$$

where $\mathbf{A}_o^+$ is the Moore-Penrose generalized inverse. Equation (63) is an under-determined algebraic system which is parameterized by generalized inversion using the Greville formula.

$$\mathbf{u}_o = \mathbf{A}_o^+(\mathbf{x}_o, t)B_o(\mathbf{x}_o, t) + \mathbf{P}_o(\mathbf{x}_o, t)\boldsymbol{\lambda}_o \quad (64)$$

where $\boldsymbol{\lambda}_o \in R^2$ is null control vector defined as $\boldsymbol{\lambda}_o = \mathbf{k}_o\dot{\mathbf{e_o}}^T$, and $\mathbf{P}_o$ is the null projection matrix for the outer loop given by

$$\mathbf{P}_o(\mathbf{x}_o, t) = \mathbf{I}_{2\times 2} - \mathbf{A}_o^+(\mathbf{x}_o, t)\mathbf{A}_o(\mathbf{x}_o, t). \quad (65)$$

The GDI based control laws given by (36) and (64) for the inner and outer loop, enforces the uniformly asymptotically stable constraint dynamics given by (30) and (57) respectively. It also provides partial closed loop stability to attitude dynamics given by (22) and positional dynamics given by (40) and (41).

4. GDI SINGULARITY AVOIDANCE

Generalized inversion has its limitation when it is applied to matrices with variable elements, in what is referred to as generalized inversion singularity. The problem arises when the inverted matrix tends to change rank, which causes discontinuity in the MPGI matrix function, and causes the elements of the MPGI matrix to go unbounded. This phenomenon is avoided in the present approach by appealing to extended GDI control, see Hameduddin and Bajodah (2012). For singularity avoidance, a first order delaying dynamic scaling factor ν_i is introduced in the particular (first) part of the GDI control law of the inner attitude loop, governed by

$$\dot{\nu}_i(t) = -\nu_i(t) + \frac{\gamma_i}{\|\mathbf{e}_i(t)\|^2}, \ \nu_i(0) > 0. \quad (66)$$

The homogeneous part of the above written first order differential equation is asymptotically stable, and γ_i in the forcing term is a positive real valued constant. Now the modified generalized inverse for inner loop is written as

$$\mathbf{A}_i^*(\mathbf{x}_i, \nu_i, t) = \frac{\mathbf{A}_i^T(\mathbf{x}_i, t)}{\mathbf{A}_i(\mathbf{x}_i, t)\mathbf{A}_i^T(\mathbf{x}_i, t) + \nu_i(t)}. \quad (67)$$

Based on this modification, the modified GDI control law for inner attitude dynamics becomes

$$\mathbf{u}_i^* = \mathbf{A}_i^*(\mathbf{x}_i, \nu_i, t)B_i(\mathbf{x}_i, \mathbf{x}_r, t) + \mathbf{P}_i(\mathbf{x}_i, t)\boldsymbol{\lambda}_i \quad (68)$$

and the resulting body rate dynamics given by (24) becomes

$$\dot{\mathbf{x}}_r = \mathbf{A}_r(\mathbf{x}_i, \mathbf{x}_r) + \mathbf{B}_r(\mathbf{x}_r)[\mathbf{A}_i^*(\mathbf{x}_i, \nu_i, t)B_i(\mathbf{x}_i, \mathbf{x}_r, t) + \mathbf{P}_i(\mathbf{x}_i, t)\boldsymbol{\lambda}_i]. \quad (69)$$

Theorem 1. Consider the closed loop systems depicted by (22) and (69). If $\theta \neq 90^\circ$ for all $t \geq 0$. then the elements of $\mathbf{A}_i^*$ are bounded for all $t \geq 0$.

Proof. Since $\theta \neq 90^\circ$ for all $t \geq 0$, it follows that the matrix $\mathbf{H}(\mathbf{x}_i)$ given by (23) always has finite elements, which implies that the two elements of $\mathbf{A}_i$ given by (34) are always finite. Also, because the homogeneous part of the first order dynamics given by (66) is asymptotically stable, it follows that

$$\lim_{t\to\infty} \nu_i(t) = \lim_{t\to\infty} \frac{\gamma_i}{\|\mathbf{e}_i(t)\|^2}. \quad (70)$$

Hence,

$$\lim_{t\to\infty}\mathbf{A}_i^*(\mathbf{x}_i,\nu_i,t)=\lim_{t\to\infty}\frac{\mathbf{A}_i^T(\mathbf{x}_i,t)}{\mathbf{A}_i(\mathbf{x}_i,t)\mathbf{A}_i^T(\mathbf{x}_i,t)+\frac{\gamma_i}{\|\mathbf{e}_i(t)\|^2}} \quad (71)$$

In reference to (71), the inverse always exists if the right side of (70) is finite and non-zero since $\mathbf{A}_i\mathbf{A}_i^T$ is non-negative definite. It remains to verify that the inverse exists for the two limit conditions

$$\lim_{t\to\infty}\nu_i(t)=\lim_{t\to\infty}\frac{\gamma_i}{\|\mathbf{e}_i(t)\|^2}=\infty,0. \quad (72)$$

If the first limit condition occurs then (71) implies that

$$\lim_{t\to\infty}\mathbf{A}_i^*(\mathbf{x_i},\nu_i,t)=\lim_{t\to\infty}\frac{\mathbf{A}_i^T(\mathbf{x_i},t)}{\infty}=\mathbf{0}_{2\times1}. \quad (73)$$

If the second limit condition occurs then (71) implies that

$$\begin{aligned}\lim_{t\to\infty}\mathbf{A}_i^*(\mathbf{x_i},\nu_i,t)&=\frac{\mathbf{A}_i^T(\mathbf{x_i},t)}{\mathbf{A}(\mathbf{x_i},t)\mathbf{A}_i^T(\mathbf{x_i},t)+0}\\&=\mathbf{A}_i^+(\mathbf{x_i},t)\end{aligned} \quad (74)$$

which implies that the control function $\mathbf{u}_i^\star$ given by (68) converges to the control function $\mathbf{u}_i$ given by (36), and hence that constraint dynamics given by (30) is asymptotically realized. Nevertheless, asymptotic realization of (30) implies that $\|\mathbf{e_i}(t)\|$ asymptotically vanishes, which contradicts the second limit condition of (72). Therefore, occurrence of the second limit condition is impossible.

The guaranteed boundedness of $\mathcal{A}_i^*$ does not imply convergence of $\|\mathbf{e_i}(t)\|$ to 0 unless the first limit condition of (72) occurs. However, satisfying this first limit condition implies from (66) that ν_i is driven unbounded, which in turns drives $\mathcal{A}_i^\star$ away from $\mathcal{A}_i^+$ and drives $\|\mathbf{e_i}(t)\|$ away from 0. Hence, selection of the scaling factor γ_i is a tradeoff between state trajectory tracking performance and generalized inversion singularity robustness, and γ_i must be tuned to achieve both satisfactory tracking performance and GDI singularity avoidance. Based on the similar approach, a dynamic scaling factor ν_o is included in the definition of MPGI matrix for the outer position loop which implies

$$\dot{\nu}_o(t)=-\nu_o(t)+\frac{\gamma_o}{\|\mathbf{e}_o(t)\|^2},\ \nu_o(0)>0 \quad (75)$$

where γ_o is the forcing term is a positive real valued constant. Now the modified generalized inverse for the outer position loop becomes

$$\mathbf{A}_o^*(\mathbf{x}_o,\nu_o,t)=\frac{\mathbf{A}_o^T(\mathbf{x}_o,t)}{\mathbf{A}_o(\mathbf{x}_o,t)\mathbf{A}_o^T(\mathbf{x}_o,t)+\nu_o(t)}. \quad (76)$$

Based on this modification, the modified GDI control law for outer position dynamics becomes

$$\mathbf{u}_o^*=\mathbf{A}_o^*(\mathbf{x}_o,\nu_o,t)B_o(\mathbf{x}_o,t)+\mathbf{P}_o(\mathbf{x}_o,t)\boldsymbol{\lambda}_o. \quad (77)$$

5. ROBUST GDI CONTROL

The conventional GDI control depends explicitly on the mathematical model of system dynamics. To make the methodology robust against unknown but bounded disturbances and modeling uncertainties, a new perspective is introduced in this paper in which GDI is combined with SMC which is well known algorithm for its inherent robustness characteristics. Define the sliding surface variables s_i and s_o for inner attitude and outer position loop as

$$s_i=\dot{\xi}_i+c_1(t)\xi_i+c_2(t)\int\xi_i dt. \quad (78)$$

$$s_o=\dot{\xi}_o+c_3(t)\xi_o+c_4(t)\int\xi_o dt. \quad (79)$$

The time derivatives of the sliding surfaces are

$$\dot{s}_i=\ddot{\xi}_i+c_1(t)\dot{\xi}_i+c_2(t)\xi_i. \quad (80)$$

$$\dot{s}_o=\ddot{\xi}_o+c_3(t)\dot{\xi}_o+c_4(t)\xi_o. \quad (81)$$

Notice that driving $\dot{s}_i$ and $\dot{s}_o$ to zero implies asymptotic realization of the constraint dynamics given by (30) and (57) respectively. Hence, let $\dot{s}_i$ and $\dot{s}_o$ are defined as

$$\dot{s}_i=\mathbf{A}_i(\mathbf{x}_i,t)\mathbf{u}_i^*-B_i(\mathbf{x}_i,\mathbf{x}_r,t) \quad (82)$$

$$\dot{s}_o=\mathbf{A}_o(\mathbf{x}_o,t)\mathbf{u}_o^*-B_o(\mathbf{x}_o,t) \quad (83)$$

and let the hybrid SMC-GDI control laws for inner and outer loop be constructed to be of the following form

$$\begin{aligned}\mathbf{u}_i^*=\ &\mathbf{A}_i^*(\mathbf{x}_i,\nu_i,t)B_i(\mathbf{x}_i,\mathbf{x}_r,t)+\mathbf{P}_i(\mathbf{x}_i,t)\boldsymbol{\lambda}_i\\&-C_i\mathbf{A}_i^*(\mathbf{x}_i,\nu_i,t)\frac{s_i}{\|s_i\|}\end{aligned} \quad (84)$$

$$\begin{aligned}\mathbf{u}_o^*=\ &\mathbf{A}_o^*(\mathbf{x}_o,\nu_o,t)B_o(\mathbf{x}_o,t)+\mathbf{P}_o(\mathbf{x}_o,t)\boldsymbol{\lambda}_o\\&-C_o\mathbf{A}_o^*(\mathbf{x}_o,\nu_o,t)\frac{s_o}{\|s_o\|}\end{aligned} \quad (85)$$

where, $C_i\mathbf{A}_i^*(\mathbf{x}_i,\nu_i,t)$ and $C_o\mathbf{A}_o^*(\mathbf{x}_o,\nu_o,t)$ are the gains to enforce sliding.

6. STABILITY ANALYSIS OF RGDI CONTROL

Theorem 2. The control law given by (84) and (85) drives the sliding surfaces s_i and s_o given by (78) and (79) to zero in finite time.

Proof. Substituting the expression of $\mathbf{u}_i^*$ given by (84) in (82) yields

$$\begin{aligned}\dot{s}_i=\mathbf{A}_i(\mathbf{x}_i,t)\{&\mathbf{A}_i^*(\mathbf{x}_i,\nu_i,t)B_i(\mathbf{x}_i,\mathbf{x}_r,t)+\mathbf{P}_i(\mathbf{x}_i,t)\boldsymbol{\lambda}_i\\&-C_i\mathbf{A}_i^*(\mathbf{x}_i,\nu_i,t)\frac{s_i}{\|s_i\|}\}-B_i(\mathbf{x}_i,\mathbf{x}_r,t).\end{aligned} \quad (86)$$

Furthermore, substituting the expression of $\mathbf{P}_i$ given by (38) in the resulting expression of $\dot{s}_i$ yields

$$\begin{aligned}\dot{s}_i=&\mathbf{A}_i(\mathbf{x}_i,t)\mathbf{A}_i^*(\mathbf{x}_i,\nu_i,t)B_i(\mathbf{x}_i,\mathbf{x}_r,t)+\mathbf{A}_i(\mathbf{x}_i,t)\mathbf{I}_{2\times2}\boldsymbol{\lambda}_i\\&-\mathbf{A}_i(\mathbf{x}_i,t)\mathbf{A}_i^+(\mathbf{x}_i,t)\mathbf{A}_i(\mathbf{x}_i,t)\boldsymbol{\lambda}_i\\&-C_i\mathbf{A}_i(\mathbf{x}_i,t)\mathbf{A}_i^*(\mathbf{x}_i,\nu_i,t)\frac{s_i}{\|s_i\|}-B_i(\mathbf{x}_i,\mathbf{x}_r,t).\end{aligned} \quad (87)$$

By recalling that the following identity holds true

$$\mathcal{A}_i(\mathbf{x}_i,t)\mathcal{A}_i^+(\mathbf{x}_i,t)=1 \quad (88)$$

for all $\mathcal{A}_i(\mathbf{x}_i,t)\neq\mathbf{0}_{1\times2}$, the expression of $\dot{s}_i$ given by (87) reduces to

$$\begin{aligned}\dot{s}_i=&\mathbf{A}_i(\mathbf{x}_i,t)\mathbf{A}_i^*(\mathbf{x}_i,\nu_i,t)B_i(\mathbf{x}_i,\mathbf{x}_r,t)\\&-C_i\mathbf{A}_i(\mathbf{x}_i,t)\mathbf{A}_i^*(\mathbf{x}_i,\nu_i,t)\frac{s_i}{\|s_i\|}-B_i(\mathbf{x}_i,\mathbf{x}_r,t).\end{aligned} \quad (89)$$

On the other hand, (88) does not hold true for $\mathcal{A}_i^*(\mathbf{x}_i,\nu_i,t)$. Nevertheless, because $\nu_i\in(0,\infty)$, it follows from (67) that

$$0<\mathcal{A}_i(\mathbf{x_u},t)\mathcal{A}_i^*(\mathbf{x_u},\nu_i,t)<1. \quad (90)$$

Therefore, (89) becomes

$$\dot{s}_i=(\delta_i-1)\mathcal{B}_i-C_i\delta_i\frac{s_i}{\|s_i\|} \quad (91)$$

where $\delta_i = \mathcal{A}(\mathbf{x}_i, t)\mathcal{A}_i^*(\mathbf{x}_i, \nu_i, t)$. Consider a positive definite candidate Lyapunov function as

$$V_i = \frac{1}{2}s_i^2. \tag{92}$$

The time derivative of V_i along the AUV system trajectories is

$$\begin{aligned}\dot{V}_i &= s_i\dot{s}_i \\ &= s_i(\delta_i - 1)\mathcal{B}_i - C_i s_i \delta_i \frac{s_i}{\|s_i\|}.\end{aligned} \tag{93}$$

Therefore, choosing C_i such that

$$C_i(\mathbf{x}_i, \mathbf{x}_r, \nu_i, t) > \frac{\delta_i - 1}{\delta_i}\mathcal{B}_i(\mathbf{x}_i, \mathbf{x}_r, t) \tag{94}$$

guarantees $\dot{V}_i$ to be negative, and hence guarantees finite time convergence of s_i to zero and finite time convergence of ξ_i to zero.

Similarly to prove stability for the outer position loop, the value of $\mathbf{u}_o^*$ given by (85) is place in (83), after simplification which yields

$$\dot{s}_o = (\delta_o - 1)\mathcal{B}_o - C_o\delta_o\frac{s_o}{\|s_o\|} \tag{95}$$

where $\delta_o = \mathcal{A}(\mathbf{x_o}, t)\mathcal{A}_o^*(\mathbf{x_o}, \nu_o, t)$. Consider a positive definite candidate Lyapunov function as

$$V_o = \frac{1}{2}s_o^2. \tag{96}$$

The time derivative of V_o along the AUV system trajectories is

$$\begin{aligned}\dot{V}_o &= s_o\dot{s}_o \\ &= s_o(\delta_o - 1)\mathcal{B}_o - C_o s_o \delta_o \frac{s_o}{\|s_o\|}.\end{aligned} \tag{97}$$

Therefore, choosing C_o such that

$$C_o(\mathbf{x}_o, \nu_o, t) > \frac{\delta_o - 1}{\delta_o}\mathcal{B}_o(\mathbf{x}_o, t) \tag{98}$$

guarantees $\dot{V}_o$ to be negative, and hence guarantees finite time convergence of s_o to zero and finite time convergence of ξ_o to zero.

7. SIMULATION RESULTS

Numerical simulations are carried out on 6DOF MBARI AUV simulator in SIMULINK/MATLAB for the following two scenarios.

7.1 Step Profile Tracking

In this scenario, reference trajectories are generated in such a way that the vehicle follows the staircase, in which two step profiles having magnitude of $50m$ and $25m$ are given in depth and east directions respectively. The positional tracking performance in 3 Dimensions (3D) is shown in Fig. 3. It is apparent from Fig. 4, that RGDI very efficiently follows the required pitch and yaw attitude trajectories in order to attain the desired positions z_{ed} and y_{ed} respectively. The elevator and rudder deflections are shown in Fig. 5, which clearly shows that the proposed control strategy provides stable tracking performance.

7.2 Helical Trajectory Tracking for Robustness Analysis

In this scenario, the AUV is commanded to follow the helical trajectory in yz_e plane under perturbed marine environment. The parametric variations together with their magnitudes are listed in table. 2. In this plot, initially the AUV is commanded to attain a depth of $30m$ then the sinusoidal trajectories is being given in z_e and y_e directions having an amplitude of $10m$ with a phase shift in order to generate the helical trajectory over the range of $10km$. An excellent positional tracking in 3D is shown in Fig. 6, which accurately tracks the given helical path with rapid convergence towards the desired values.The tracking of pitch and yaw attitude profiles, required to follow the helical trajectory is shown in Fig. 7. The control deflections are shown in Fig. 8 which is very much realizable.

Table 2. Parametric variations

Parameters	Nominal value	Perturbed value
$L\ (m)$	5.554	6.105
$m\ (kg)$	1093.1	907.56
$x_b\ (cm)$	12.09	14.0
$x_g\ (cm)$	12.09	14.0
$z_g\ (cm)$	0.65	0.70
$I_x\ (kg.m^2)$	36.677	54.698
$I_y\ (kg.m^2)$	2154.3	2270.4
$I_z\ (kg.m^2)$	2154.3	2270.4
X_{uu}	-23.5	-23.2
Y_{uu}	-920.1	-872.1
Z_{uu}	-920.1	-813.4

8. CONCLUSION

This paper presents the design of RGDI based autopilot for position and attitude control of AUV. A two-loop structured control using RGDI is proposed, in which dynamic constraints are defined successfully in the framework of GDI and its inverse is calculated by incorporating MPGI based Greville formula. The outer loop successfully generates the desired pitch and yaw attitude profiles based on

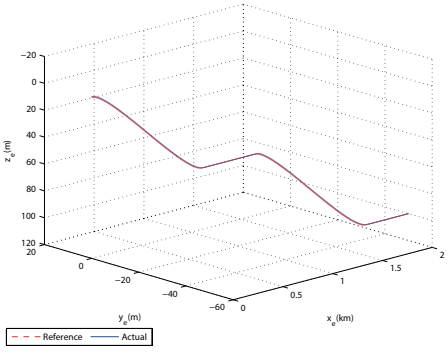

Fig. 3. Position tracking in 3D vs. time

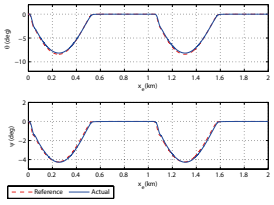

Fig. 4. Angles vs. time

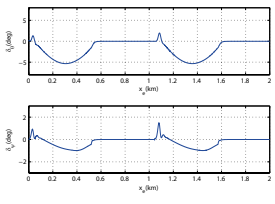

Fig. 5. Deflections vs. time

positional errors in depth and east directions respectively. The inner loop is responsible for precise attitude tracking required to minimize the positional errors. A dynamic scaling factor is augmented to address the singularity problem successfully. The robustness is ensured by augmentation of SMC based robust term in the framework of GDI. To validate the performance of RGDI, numerical simulations are conducted on MBARI AUV simulator, developed in SIMULINK/MATLAB. The overall stability of RGDI is ensured by using Lyapunov based energy function that provides stable tracking while maintaining vehicle stability. Simulation results show that the RGDI based controller is effective and robust, by providing better trajectory tracking and not influenced by external disturbances and parametric variations due to marine environment.

REFERENCES

Bajodah, A. (2009a). Asymptotic perturbed feedback linearisation of underactuated euler's dynamics. *International Journal of Control*, 82(10), 1856–1869.

Bajodah, A. (2009b). Generalised dynamic inversion spacecraft control design methodologies. *IET control theory & applications*, 3(2), 239–251.

Bajodah, A. (2010). Asymptotic generalised dynamic inversion attitude control. *IET Control Theory & Applications*, 4(5), 827–840.

Ben-Israel, A. and Greville, T.N. (2003). *Generalized inverses: theory and applications*, volume 15. Springer Science & Business Media.

Chowdhury, A.R., Vishwanathan, V., Prasad, B., Kumar, R., and Panda, S. (2014). Inverse dynamics control of a bio-inspired robotic-fish underwater vehicle propulsion based on lighthill slender body theory. In *OCEANS 2014-TAIPEI*, 1–6. IEEE.

Das, B., Subudhi, B., and Bhusan Pati, B. (2014). Adaptive sliding mode formation control of multiple underwater robots. *Archives of Control Sciences*, 24(4), 515–543.

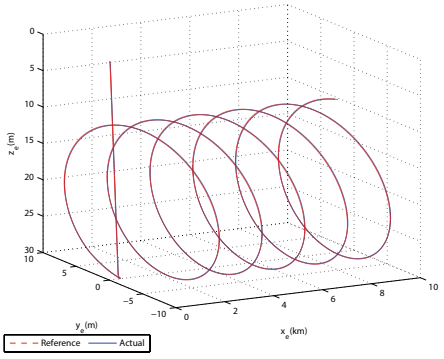

Fig. 6. Position tracking in 3D

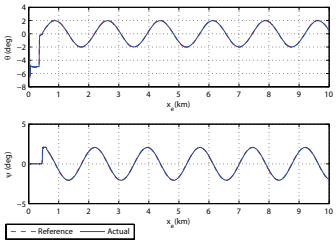

Fig. 7. Angles vs. time

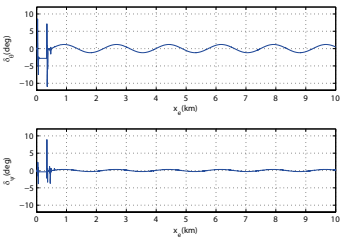

Fig. 8. Deflections vs. time

Eski, I. and Yildirim, S. (2014). Design of neural network control system for controlling trajectory of autonomous underwater vehicles. *International Journal of Advanced Robotic Systems*, 11.

Gui, H., Jin, L., and Xu, S. (2013). Attitude maneuver control of a two-wheeled spacecraft with bounded wheel speeds. *Acta Astronautica*, 88, 98–107.

Hameduddin, I. and Bajodah, A.H. (2012). Nonlinear generalised dynamic inversion for aircraft manoeuvring control. *International Journal of Control*, 85(4), 437–450.

Khodayari, M.H. and Balochian, S. (2015). Modeling and control of autonomous underwater vehicle (AUV) in heading and depth attitude via self-adaptive fuzzy PID controller. *Journal of Marine Science and Technology*, 1–20.

Kim, M., Joe, H., Kim, J., and Yu, S.c. (2015). Integral sliding mode controller for precise maneuvering of autonomous underwater vehicle in the presence of unknown environmental disturbances. *International Journal of Control*, (just-accepted), 1–43.

Lakhekar, G., Waghmare, L., and Londhe, P. (2015). Enhanced dynamic fuzzy sliding mode controller for autonomous underwater vehicles. In *Underwater Technology (UT), 2015 IEEE*, 1–7. IEEE.

McEwen, R. and Streitlien, K. (2001). Modeling and control of a variable-length AUV. *Proc 12th UUST*.

Nelson, R.C. (1998). *Flight stability and automatic control*, volume 2. WCB/McGraw Hill.

Prestero, T.T.J. (2001). *Verification of a six-degree of freedom simulation model for the REMUS autonomous underwater vehicle*. Ph.D. thesis, Massachusetts institute of technology.

Steinicke, A. and Michalka, G. (2002). Improving transient performance of dynamic inversion missile autopilot by use of backstepping. In *AIAA Guidance, Navigation, and Control Conference and Exhibit, Monterey, CA*.

Subudhi, B. and Atta, D. (2009). Design of a path following controller for an underactuated auv.

Wang, Z., Liu, L., Wang, Y., and Wang, Z. (2012). Dynamic integral sliding mode for launch vehicle attitude control system. In *Control and Decision Conference (CCDC), 2012 24th Chinese*, 1713–1718. IEEE.

Xu, Y., Pang, Y., Gan, Y., and Sun, Y. (2006). AUV state of the art and prospect. *CAAI Transactions on Intelligent Systems*, 1(1), 9–16.

Xu, Y. and Xiao, K. (2007). Technology development of autonomous ocean vehicle. *Acta automatica sinica*, 33(5), 518.

Yang, I., Byun, S., Seo, B., Lee, D., and Han, D.S. (2013). Robust dynamic inversion based on sliding mode control for autonomous underwater vehicles. In *Intelligent Autonomous Vehicles*, volume 8, 79–84.

Yildiz, Ö., Gökalp, R.B., and Yilmaz, A.E. (2009a). A review on motion control of the underwater vehicles. In *Electrical and Electronics Engineering, 2009. ELECO 2009. International Conference on*, II–337. IEEE.

Yildiz, O., Yilmaz, A.E., and Gokalp, B. (2009b). State-of-the-art system solutions for unmanned underwater vehicles. *sensors*, 1, 2.